**Proceedings of the ASME 2010 3rd Joint US-European Fluids Engineering Summer Meeting and 8th International Conference on Nanochannels, Microchannels, and Minichannels
FEDSM-ICNMM2010
August 1-5, 2010, Montreal, Canada**

FEDSM-ICNMM2010-30550

EFFECT OF NANOPARTICLES ON THE SPREADING OF BUBBLE TRIPLE LINE ON TOP OF A STAINLESS STEEL SUBSTRATE NOZZLE

Saeid Vafaei
School of Engineering and Materials Science,
Queen Mary University of London
London, UK.

Dongsheng Wen
School of Engineering and Materials Science,
Queen Mary University of London
London, UK.

ABSTRACT

The purpose of this study is to investigate the effect of gold nanofluid on the formation of gas bubbles on top of a stainless steel substrate plate nozzle. The experiment reveals a unique phenomenon of enhanced pinning of the triple line of gold nanofluids for bubbles forming on the substrate plate, i.e the gold nanoparticles are found to prevent the spreading of the triple line during the bubble formation. Different to the liquid droplet measurement, the bubble contact angle is found to be slightly larger for formation of bubbles inside gold nanofluids. It is also observed that bubbles develop earlier inside the nanofluids with reduced bubble departure volume and increased bubble formation frequency. The shape of the bubble is found to be in good agreement with predictions of the Laplace-Young equation under the low gas flow rates inside water. Such a good agreement is also observed for bubbles forming inside nanofluids except a few characteristic points. The variation of solid surface tensions and the resultant force balances at the triple line are believed to be responsible for the modified dynamics of the triple line inside gold nanofluids and subsequent bubble formation.

INTRODUCTION

Since the spreading of liquids on solid substrates is of interest to many practical applications and industrial processes (such as coating, boiling and condensation, etc.), extensive experimental investigations and theoretical work have been performed in the past to understand, model and predict the shape of interfaces formed between liquids and solid surfaces of various geometrical configurations. At equilibrium, a force balance method is usually proposed at the triple line to relate the macroscopic contact angle with material properties (see Figure 1). A classical example is the Young's equation, which is typically written as

$$\sigma_{\lg} \cos\theta = \sigma_{sg} - \sigma_{sl} \qquad (1)$$

where θ is equilibrium contact angle and $\sigma_{\lg}$ is liquid-gas surface tension, which is tabulated and is widely available for a variety of materials. On the other hand, the solid-gas, σ_{sg}, and solid-liquid surface tensions, σ_{sl}, are not easily available compared to liquid-gas surface tension. Several independent approaches have been employed to estimate solid surface tensions, such as through direct force measurement, contact angles, capillary penetration into columns of particle powder, sedimentation of particles, solidification front interaction with particles, film flotation, gradient theory, Lifshitz theory and van der Waals forces, and the theory of molecular interactions [1-3].

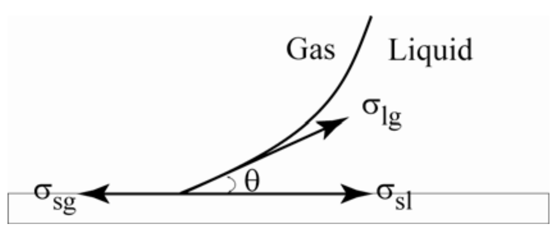

Figure 1 Schematic of solid/gas, solid/liquid, and gas/liquid surface tensions at triple line.

The mechanisms of wetting behavior of pure liquid on the solid are still not completely revealed, the introduction of nanoparticles into a base liquid, or termed as nanofluids, make it more complicated. Many experimental studies have been conducted to understand and identify the mechanisms of the effects of nanoparticles on contact angles [4-8], and surface tension [9-10].

The purpose of this study is to reveal the influence of a well-defined gold nanofluid on the spreading and pinning behavior of the triple line during the formation of gas bubbles on top of a stainless steel plate, and to compare the result with that of the numerical solution of the Laplace equation.

EXPERIMENTAL SETUP

Figure 2 illustrates the schematics of the experimental setup. The stainless steel substrate plate (0.4 mm internal diameter) is submerged into a transparent square-sized glass container of the size of 20 by 20 mm and a height of 72 mm. Figure 3 shows the dimension of stainless steel substrate plate nozzle. The stainless steel substrate is polished (R_a = 0.021 with of R_z = 0.03 μm) after drilling substrate. The glass container is filled with quiescent deionized water or gold nanofluids to a height of 20 mm and open to the atmosphere under ambient conditions. The gas flow is supplied by compressed air in a cylinder, which is connected to a high-accurate gas flow controller through a pressure reduction valve. The gas is controlled in the range of 0.015-0.83 ml/min with an accuracy of $\pm 0.5\%$ of its reading. Detailed bubble formation, especially the dynamics of triple line, are captured by a high speed camera (1200 frame/sec) equipped with an optical microscope head.

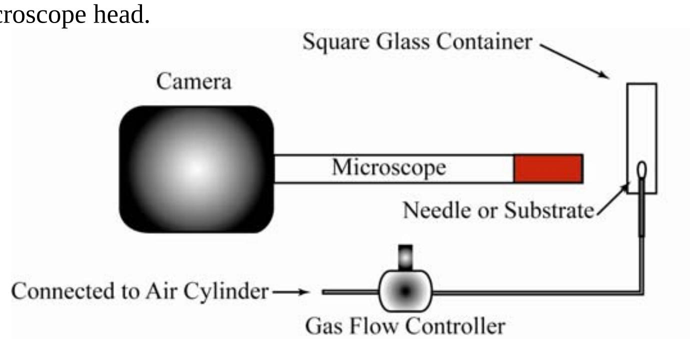

Figure 2. Schematic of the experimental setup.

Well-defined gold nanoparticles (see Figure 4), with a narrow size distribution and an average diameter of 5 nm, are dispersed into deionized water without any surfactants inside nanofluids or on the nanoparticles. To ascertain that there is no surfactant or any impurities inside gold nanofluids, a drop of nanofluids is left to be dried slowly on top of a stainless steel substrate and the chemical elements of dried nanofluid droplet are analyzed by an Energy Dispersive x-ray Spectrometer.

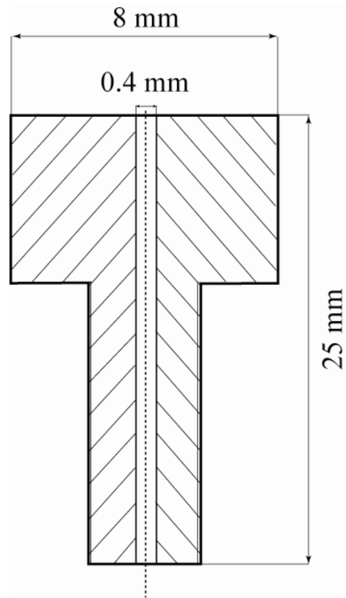

Figure 3. Dimensions of stainless steel substrate.

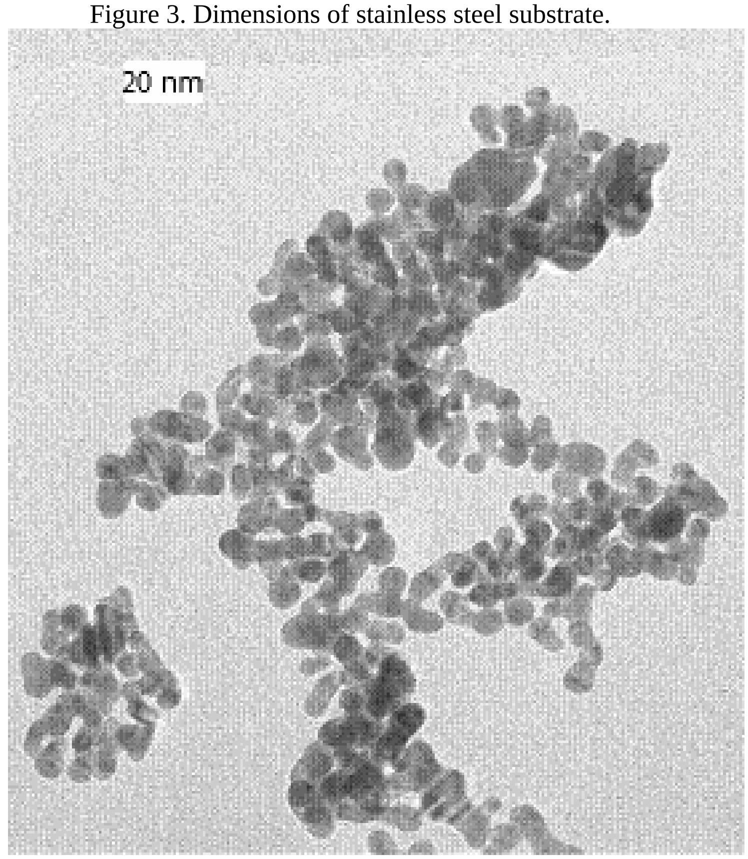

Figure 4. TEM samples of gold nanoparticles.

The result confirms the purity of gold nanofluids. The nanoparticle concentration of nanofluid is controlled at 0.01% by weight. The captured images of bubble formation are imported into the software of a Drop Shape Analysis System to measure the surface tension of gold nanofluid and water. The accuracy of surface tension measurement of device is 0.01mN/m. The nanofluid and water surface tensions are measured, using six different bubble images. The surface tension of water and nanofluid were respectively 0.07238 ± 0.0041 and 0.06753 ± 0.0066 N/m.

THEORETICAL ANALYSIS OF AXISYMMETRIC BUBBLE SHAPE

For small flow rates as in the experiments, bubble formation takes place in a quasi steady state manner, i.e. a force balance is reached between the surface tension and external forces. Mathematically, the Young-Laplace equation represents a mechanical equilibrium condition between two fluids separated by an interface. The Young-Laplace equation shows that the pressure difference across the interface is equal to the product of the curvature multiplied by the gas-liquid surface tension. Assuming that the bubble is growing in a quasi-steady state, the Young-Laplace equation on the interfacial surface can be written as

$$\Delta p = \left(\frac{1}{R_1} + \frac{1}{R_2}\right)\sigma_{lg} \qquad (4)$$

where R_1 and R_2 are the radii of curvatures, i.e. R_1 is the radius of curvature describing the latitude as it rotates and R_2 is the radius of curvature in a vertical section of the bubble describing the longitude as it rotates. The center of R_1 and R_2 are on the same line but different location. Δp is the pressure difference between the gas, p_g, and liquid phase, p_l, which can be written as

$$p_g(z) = \frac{2\sigma_{lg}}{R_o} + P_o + \rho_g gz + \rho_l gh \qquad (5)$$

$$p_l(z) = P_o + \rho_l g(h + z) \qquad (6)$$

$$R_1 = ds/d\theta \text{ and } R_2 = r/\sin\theta \qquad (7)$$

where P_o is the ambient pressure, h is the hydrostatic head and θ is the running angle. Substituting equations (5-7) into equation (4), the Young-Laplace equation is obtained as

$$\frac{d\theta}{ds} = \frac{2}{R_o} - \frac{gz}{\sigma_{lg}}(\rho_l - \rho_g) - \frac{\sin\theta}{r} \qquad (8)$$

The Young-Laplace equation can be solved, with the following system of ordinary differential equations for axisymmetric interfaces, to obtain the bubble shape.

$$\frac{dr}{ds} = \cos\theta \qquad (9)$$

$$\frac{dz}{ds} = \sin\theta \qquad (10)$$

$$\frac{dV}{ds} = \pi r^2 \sin\theta \qquad (11)$$

This system of ordinary differential equations avoids the singularity problem at the bubble apex, since

$$\left.\frac{\sin\theta}{r}\right|_{s=0} = \frac{1}{R_o} \qquad (12)$$

Knowing two parameters of a bubble shape (such as contact angle, radius of contact line, bubble volume, or location of the apex), the system of ordinary differential equations (8-11) can be solved to obtain the axisymmetric bubble shape, using the following boundary conditions [11].

$$r(0) = z(0) = \theta(0) = V(0) = 0 \qquad (13)$$

In this study, the accurately determined experimental value of the radius of contact line and the height of bubble are used as the only two inputs to solve above equations at each step time of bubble formation to predict the bubble shape and other parameters of the bubble. The accuracy of measurement of radius of contact line and bubble height is 5 μm and percentage error of calculation is $\pm 1.5\ \mu m$.

The set of first-order differential equations are solved in Version 7 of Matlab environment using the 4th order Runge-Kutta method.

The simultaneous bubble volume expansion rate is also calculated by solving Young-Laplace equation to predict the variation of bubble volume over time. The average gas flow rate is calculated by multiplying the bubble frequency and detached bubble volume, $Q_{av} = fV$. The detached bubble volume is the summation of last bubble volume predicted by Young-Laplace equation and extra volume added during detachment period, $\int_{t_l}^{t_d} Q\,dt$. The detachment time, t_d, is obtained from experiments.

RESULTS AND DISCUSSIONS

The validity of the Young-Laplace equation can be satisfied up to the detachment period, where the bubble has almost the maximum volume and would depart by supplying further gas amount or introducing small perturbations around the bubble. In the last milliseconds closing to the departure, the bubble start being stretched and consequently the viscosity plays an important role. Such a good agreement before the bubble departure is expected for bubble formation under low flow rate conditions as the gas-liquid shear stress becomes negligible. As gas flow rate increases, the increase of gas-liquid shear stress could invalidate the Young-Laplace equation, which deserves further investigation. Figure 6 compares the Young-Laplace prediction of bubble shape inside 5 nm gold nanofluid (10E-4 w) and pure water with experimental data on top of stainless steel substrate plate of 0.4 mm diameter nozzle for average gas flow rate of 0.59-0.66 ml/min. It is observed an excellent agreement between prediction of the Laplace-Young equation and experimental data inside pure water during of whole bubble formation before detachment time. This agreement also is observed for formation of bubble inside nanofluid except certain periods of time, i.e the period when the contact angle reaches to the minimum and start being increased again for formation of bubble. Figure 7 shows the detailed comparison at the vicinity of the triple line in gold nanofluid (10E-4 w) between the predictions of Young-Laplace and experimental data for an average gas flow rate of 0.66 ml/min at t=0.75 sec. Good agreement is reached and only a small difference is observed in the vicinity of solid substrate. However it is worthwhile to emphasis again here that the numerical prediction is based on two experimental inputs: the radius of the contact line and the bubble height.

More interestingly, detailed observation reveals a unique pinning behavior for bubbles forming on the substrate plate nozzles inside gold nanofluids, as shown in Figure 8. For bubbles forming inside pure water, the triple line expands rapidly at the small bubble volume, reaching a peak value of r_d~ 0.26mm at a bubble volume ~$1 \times 10^{-9} m^3$. Subsequently the radius of the contact line starts shrinking, fixed at two radius, 0.25mm and 0.24 mm (2-stage pinning), during the most of bubble growth period until a rapid shrinking at the maximum bubble volume, i.e. necking and departure period. Compared to the pure water case, a similar general trend is also observed for bubbles forming in gold nanofluids but with a few distinguish differences: a) the maximum radius of the contact line is smaller; i.e 0.235 mm; b) only one-stage pinning is observed, and the pinned radius is smaller, i.e at rd~0.23mm and c) the bubble departure at smaller bubble volume. Such an observation shows an enhanced pinning behavior of the triple line for bubbles forming inside gold nanofluids. It appears that the presence of gold nanoparticles push the triple line towards the gas side, and increase effectively the wet area, as well as promoting an early bubble departure at smaller volume.

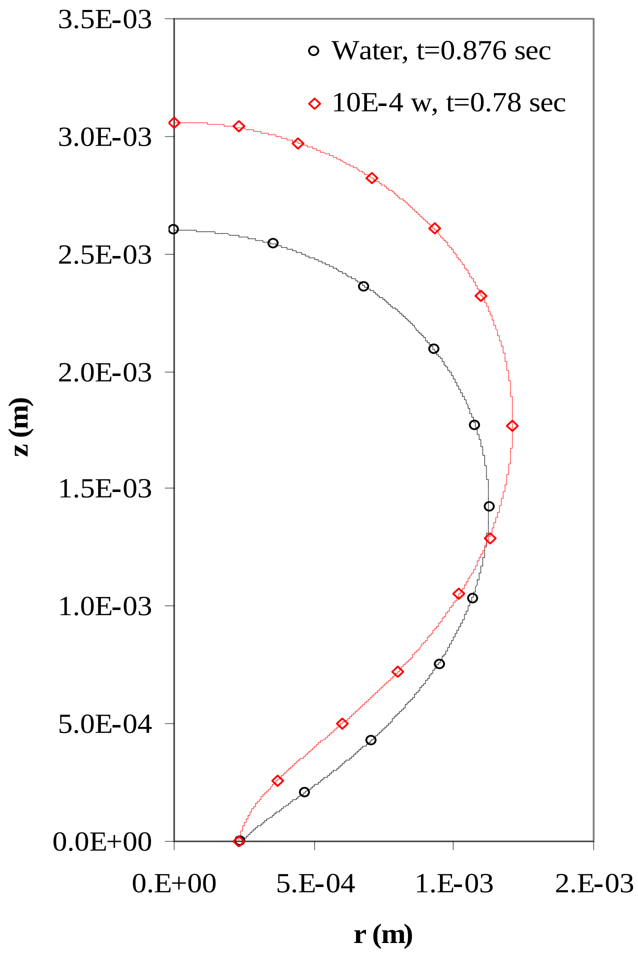

Figure 6. Comparison of experimental bubble shape and prediction of Young-Laplace equation on top of stainless steel substrate plate nozzle of 0.4 mm diameter, $Q_{av} \approx 0.59 - 0.66\, ml/\min$.

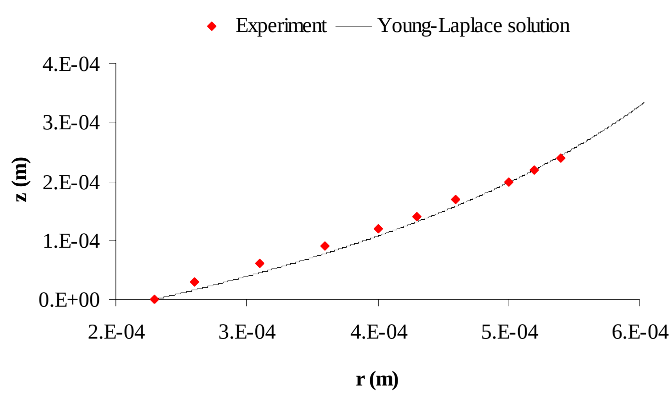

Figure 7. Comparison of experimental nanofluid (10E-4 w) bubble shape and prediction of Young-Laplace equation on top of stainless steel substrate plate nozzle of 0.4 mm diameter at t=0.75 sec and $Q_{av} = 0.66\, ml/\min$.

The variation of the contact angle, radius of contact line with bubble volume inside water and gold nanofluids on top of stainless steel substrate plate nozzle can be observed in Figure 8. The bubble contact angle inside water and nanofluids experiences a general decrease and then increase period. The decrease period is not monotonic but a step-wise. As bubble volume increases, the contact angle decreases, and radius of contact line rapidly increases. As the effect of buoyancy becomes dominant by increasing of bubble volume, the entire bubble start being pushed up, therefore the contact angle began to increase and as bubble developing upward, and the radius of contact line decreases. The maximum radius of contact line depends on forces that acting on the triple line. The bubble will be developing upward until reaches to the necking and departure stages. It is observed that the minimum contact angle is smaller inside nanofluid due to the presence of gold nanoparticles. The contact angle is nearly identical inside nanofluids and pure water before the minimum value for a given volume. After that, the difference increases as the effect of buoyancy force becomes more effective. The bubble contact angle inside nanofluids is found to be slightly higher for a given bubble volume.

Separate experiments on the wetting behavior show that the contact angle of gold nanofluid droplet on the stainless steel substrate is smaller than that of pure water for a given droplet volume, a strong indication of improved wettability. However, as analyzed above, the instantaneous contact angle during bubble formation inside the gold nanofluids is larger than that inside pure water for a given volume. This suggests that the overall enhancement in wettablity for gold nanofluids is caused by a strong pinning behavior, which also affects the instantaneous contact angle value. The variation of solid surface tensions is expected to be responsible for modification of pinning behavior of triple line in the presence of nanoparticles (see Figure 1). The specifications of stainless steel substrates such as homogeneity and solid surface roughness for bubble and droplet contact angle measurement were similar.

In addition, it is observed that the average gas flow rate, $Q_{av} = fV$, inside nanofluids is higher than that of water for a given nominal gas flow rate, i.e values specified at the gas flow rate controller. Other experiments show that such a difference is small for bubbles forming on top of a stainless steel needle nozzle. Under both cases, the bubble departure volume is larger for bubbles forming inside water. From a quasi-equilibrium force analysis, the downward surface tension force increases by the increase of surface tension, radius of contact line and contact angle. The gold nanoparticles appear playing dual roles on the average gas flow rate. The presence of gold nanoparticles decreases the radius of contact line; however the resultant slight decrease in surface tension increases the contact angle. A decrease in surface tension also reduces the capillary pressure, which would reduce the bubble formation time and increase the bubble departure frequency. The average gas flow rate depends on a combination of these factors.

Figure 9 shows the relationship of bubble height, radius of curvature at apex, and radius of contact line with time on top of stainless steel substrate plate inside water and gold nanofluids. The variation of radius of contact line affects the variation of bubble height and radius of curvature at apex. The pinning behavior of triple line inside water and nanofluids can be observed in Figures 8, and 9. Such an observation clearly illustrates that the dominant effect of nanoparticles lies on the triple line.

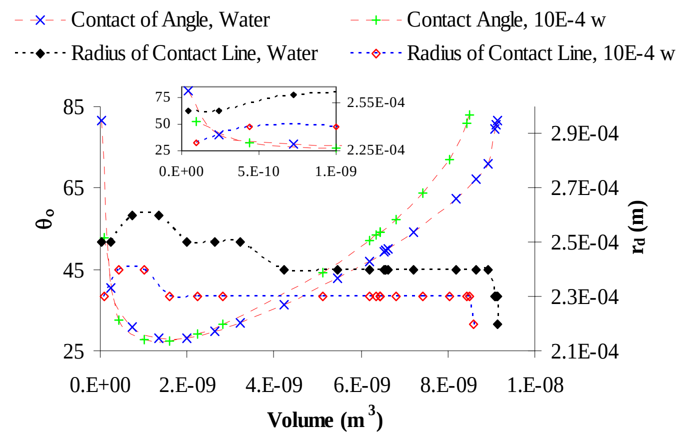

Figure 8. Variation of radius of contact line and contact angle with volume on top of stainless steel substrate plate inside water and 10E-4 w gold nanofluids, $Q_{av} = 0.56 - 0.66\, ml\ / \min$.

All these experimental results demonstrate a strong promotion of pinning behavior of the triple line by introducing gold nanoparticles, which modify significantly the bubble dynamics. As it is known that for boiling heat transfer and the occurrence of the critical heat transfer where the evaporation of microlayers underneath the bubbles or around dry spots is the major influencing factor, the modification of the dynamics of the triple line by nanoparticles will have a strong effect. The influence of nanoparticles on contact line has been reported through experiments conducted on liquid meniscus and droplets on a hot plate [12]. However, it is worthwhile to emphasis the difference to other observations on pool boiling of nanofluids as reported [10, 13-14], which were ascribed to the effects of nanoparticle deposition and consequent modification of boiling surfaces forming a coating or porous layer, there is no heating in our experiments, and the gold nanofluids are stable with nearly uniform size distribution centered around 5 nm and with negligible particle deposition effects.

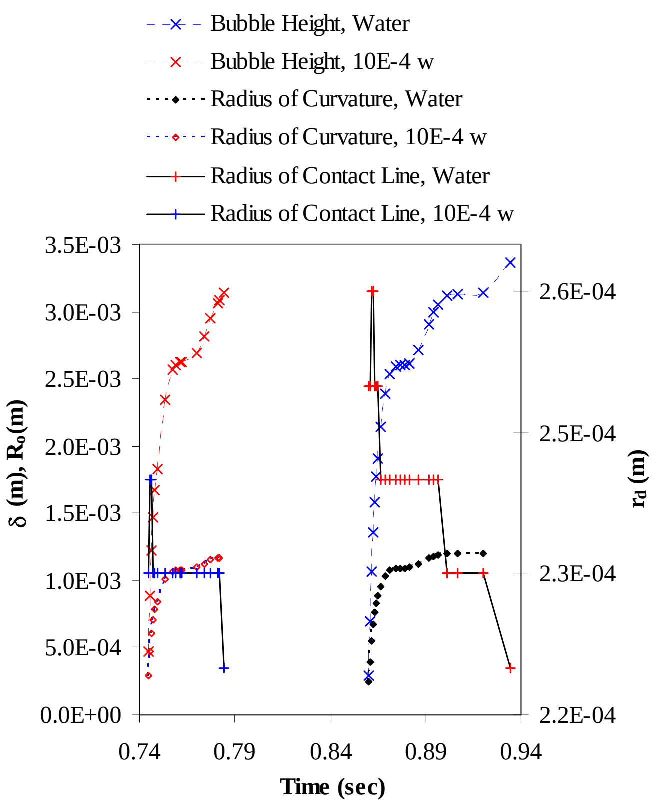

Figure 9. Variation of radius of contact line at apex, bubble height, and radius of contact line with time inside water and nanofluids, $Q_{av} = 0.56 - 0.66\ ml / \min$.

However, well-built promotion of pinning behavior of triple line and an increase of contact angle of bubble at the same bubble volume compared to pure water is observed. The location of pinning of triple line on the top of stainless steel needle (somewhere in middle of wall thickness) is observed by SEM after experiment to make sure, these effect are not coming from particle deposition effects.

The reasons for such promoted pinning behavior at the triple line associated with a slight increase in the contact angle at the late stage of bubble growth are still not completely clear. The previously mentioned structural disjoining pressure could not fully account for it due to the low particle concentrations. Adding particles into pure liquid would cause interactions with liquid molecules, particles and also the solid surfaces, which are the main cause of different properties and behavior of the collective dispersion system. A quantitative description of the wettability requires detailed information about the spreading parameter, S, where $S = \sigma_{sg} - \sigma_{sl} - \sigma_{\lg}$, and the dynamics of the triple line is dependent upon the force balance, as shown in Figure 1. Obviously, the solid-gas, solid-liquid, and liquid-gas surface tensions will have a significant role on the spreading of triple line, contact angle and the promotion of pinning of triple line. In addition, the surface homogeneity and roughness of substrate could be important on the variation of contact angle [15-19]. The effect of surface roughness can be considered using Wenzel equation, $\cos\theta_w = r\cos\theta$, where r is roughness and defined as a ratio of real to projected area. The roughness of a surface further decreases the contact angle if the contact angle is < 90°, whereas the roughness further increases the contact angle if the contact angle is > 90°. An increase in the surface roughness will increase the actual substrate area that contributes to the overall liquid-solid interaction.

Since the sedimentation of nanoparticles of nanofluids is not observed during the experiment, the variation of surface roughness and homogeneity is expected not to be much [20]. As a consequence, it is likely that the observed dynamics of the triple line is related to the variation of the solid surface tensions due to the presence of nanoparticles and consequently, a promotion of the pinning behavior of triple lines.

CONCLUSIONS

This work shows that well-defined nanofluids can affect significantly bubble formation on a substrate plate, which includes

a) An improvement of the wetting capability by nanofluids is clearly illustrated, which promotes the pinning behavior of the triple line and contribute to the departure of bubbles.

a) A similar general trend of the variation of contact angle is observed inside pure water and gold nanofluids; however, the minimum bubble contact angle inside the nanofluids becomes smaller due to the presence of gold nanoparticles. The bubble contact angle inside gold nanofluids is slightly higher under the same bubble volume.

b) The promoted pinning behavior of the triple line is believed to be associated with the modification of solid surface tensions, and be responsible for the rising bubble contact angle for a given volume.

c) Using experimental captured bubble height and the radius of contact line as two input parameters, the Young-Laplace equation can predict the bubble shape quite well in pure water. Good agreement is also reached for bubble growth inside nanofluids apart from a few characteristic points.

ACKNOWLEDGMENTS

The authors are grateful for the financial support of EPSRC under the grant number EP/E065449/1ut acknowledgments here.

REFERENCES

[1] Spelt J. K., Li D., The equation of state approach to interfacial tensions, in: Neumann A. W., Spelt, J. K. Eds., Applied Surface Thermodynamics, Marcel Dekker Inc., New York, 1996, pp. 239-292.

[2] Matyushov, D. V., Schmid, R., J. Chem. Phys., 1996, 104, 8627.

[3] Kwok, D. Y.; Neumann, A. W., Advances in Colloid and Interface Science 1999, 81, 167.

[4] Vafaei, S; Borca-Tasciuc, T.; Podowski, M. Z.; Purkayastha, A.; Ramanath, G.; Ajayan, P.M., Nanotechnology 2006, 17, 2523.

[5] Sefiane, K.; Skilling, J.; MacGillivray, J., Advances in Colloid and Interface Science 2008, 138, 101.

[6] Vafaei, S.; Wen, D; Ramanath, G.; Borca-Tasciuc, T.,11th International Symposium on Gas-Liquid Two-Phase Flows, ASME, August 2-5, 2009, Vail, Colorado, USA.

[8] Coursey, J. S.; Kim, J., International Journal of Heat and Fluid Flow 2008, 29, 1577.

[9] Kim, S. J.; Bang, I. C.; Buongiorno, J.; Hub, L. W., International Journal of Heat and Mass Transfer 2007,50, 4105.

[10] Vafaei, S.; Purkayastha, A; Jain, A.; Ramanath, G.; Borca-Tasciuc, T., Nanotechnology 2009, 20, 185702.

[11] Neumann A.W., Spelt J. K., Applied Surface Thermodynamics, M. Dekker, 1996.

[12] Sefiane, K., Applied Physics Letters 2006,89, 044106.

[13] Kim, S. J.; McKrell, T.; Buongiorno, J.; Hu, L. W., Journal of Heat Transfer 2009, 131, 043204.

[14] Kim, S. J., Bang, I. C., Buongiorno, J., Hu, L. W., Applied Physics Letters 2006, 89, 153107.

[15] Cassie, A. B. D. Discuss. Faraday Soc., 1948, 3, 11.

[16] Baxer, S., Cassie, A. B. D., Journal of Text Inst., 1945, 36T, 67.

[17] Cassie, A. B. D., Baxter, S.,Trans. Faraday Soc.,1944, 40, 546.

[18] Wenzel R. N., Ind Engineering chemical, 1936, 28, 988.

[19] Wolansky G., Marmur A., Colloids and Surfaces A: Physicochemical and Engineering Aspects, 1999, 156, 381.

[20] Kim, S. J., McKrell, T., Buongiorno, J., Hu, L. W., Journal of Heat Transfer, 2009,131, 0432041.

